Hindawi
Shock and Vibration
Volume 2019, Article ID 3402084, 12 pages
https://doi.org/10.1155/2019/3402084

Research Article

Hopf Bifurcation Characteristics of the Vehicle with Rear Axle Compliance Steering

Xiaomei Xu,[1] **Dong Chen**,[2] **Lei Zhang**,[1] **and Ning Chen**[2]

[1]*College of Automobile and Traffic Engineering, Nanjing Forestry University, Nanjing 210037, China*
[2]*College of Mechanical and Electronic Engineering, Nanjing Forestry University, Nanjing 210037, China*

Correspondence should be addressed to Ning Chen; chenning@njfu.com.cn

Received 8 July 2018; Revised 28 October 2018; Accepted 30 December 2018; Published 28 January 2019

Academic Editor: Mario Terzo

To overcome the shortage of traditional rear axle compliance steering (RACS) technology, a kind of viscoelastic smart material is introduced into the rear suspension of a vehicle to construct rear wheel semiactive steering system. This article focuses on the nonlinear dynamic behavior of the vehicle with RACS incorporating viscoelastic smart material. First of all, considering the tire nonlinearity and the fractional derivative constitutive relation of the viscoelastic material, the nonlinear dynamic model of the vehicle with RACS is formulated. Then, the lateral dynamic behavior of the vehicle with RACS is demonstrated through numerical experiments. Finally, some factors that influence shimmy of the compliance steering wheel are investigated. Numerical results demonstrate the Hopf bifurcation characteristics of the vehicle with RACS and disclose the influence factors of Hopf bifurcation characteristics for the vehicle with RACS, which lay the theoretical foundation for the development of the rear wheel semiactive steering technology.

1. Introduction

It is well known that four-wheel steering technology can improve vehicle lateral stability at middle or high speeds through making the rear wheels turn to the same direction as that of the front wheels [1]. There are mainly two kinds of rear wheel steering modes: one is the rear wheel active steering (RWAS) and the other is the rear wheel passive steering which is also called rear axle compliance steering (RACS). RWAS can make the vehicle achieve good lateral stability in wide speed range; however, its steering system is complex and the reliability is not high [2]. RACS utilizes the tire lateral force and the lateral elasticity of the rear suspension to make the rear axle turn a small angle relative to the vehicle body [3]. Because the compliance steering stiffness is constant, RACS has effect on improving the vehicle lateral stability only in narrow speed range. Compared with RWAS, however, RACS has simpler structure and better reliability.

Traditional RACS technology focuses on how to rationally use the compliance characteristics of the rear suspension [4]. In recent years, more and more smart material has been developed, such as magnetorheological fluid (MRF), magnetorheological elastomer (MRE), memory alloy, electrostrictive material, and piezoelectric material [5]. The MR damper has been successfully applied to the vehicle suspension to actualize semiactive control of the damping force, which makes up for the deficiency of the passive suspension [6]. Moreover, compared with the active suspension, the semiactive suspension with MR damper is lower in energy consumption and simpler in structure. For this reason, the smart material is also considered to be introduced into the rear suspension to actualize rear wheel semiactive steering. Xu et al. [7] introduced the smart material into the rear suspension to construct rear wheel semiactive steering system and analyzed the technical feasibility in theory based on the linear dynamic model. However, vehicle itself is a complex dynamic system and it includes many nonlinear parts. Moreover, smart material itself has complex material properties. Therefore, the vehicle with RACS incorporating smart material is a complex nonlinear dynamic system. The nonlinear dynamic system will lead to nonlinear dynamic behavior, such as wheel shimmy or vehicle body shimmy.

The problems about wheel shimmy or vehicle body shimmy have been widely studied, and a great deal of beneficial achievements has been used to attenuate vehicle shimmy. Many research studies on the occurrence mechanism of vehicle shimmy have also been carried out. Lu et al. [8] investigated the global response of vehicle shimmy system with multiclearance joints by using the point mapping method and analyzed the dynamic mechanism for vehicle shimmy based on energy input. Ran et al. [9] adopted linear and nonlinear techniques, including bifurcation analysis, to analyze the shimmy stability of a trailing wheel suspension system and evaluate the differences between tire models. They found that although the nonlinear tire models did not change the stability of equilibria, they determined the magnitude of the oscillation. Dutta and Choi [10] designed a new type of adaptive sliding mode controller which could settle effectively the problem of steering motion near the equilibrium position and reduced the wheel shimmy motion by a considerable amount. Mi et al. [11] investigated the model establishment and parameter analysis on shimmy of the electric vehicle with independent suspensions. They conducted the stability charts for the electric vehicle and found that bifurcation occurred at certain vehicle forward speed and the suspension structural parameters affected wheel shimmy.

There is no doubt that the research mentioned above is beneficial for understanding the occurrence mechanism of vehicle shimmy and is helpful to attenuate vehicle shimmy. However, considering the nonlinear characteristics of tires, it is still necessary to carry out research studies on the nonlinear dynamic behavior of the vehicle with RACS incorporating smart material. Smart materials with large parameters regulating range are usually viscoelastic materials. Properties of this kind of viscoelastic material can be well depicted with fractional derivative constitutive relation [12]. Therefore, the fractional order model of RACS incorporating viscoelastic material was firstly proposed in this study, and then, the nonlinear dynamic model of the vehicle with RACS was formulated. Hopf bifurcation characteristics of the vehicle with RACS were investigated through numerical experiments. Some factors contributing to shimmy phenomenon of the vehicle with RACS were analyzed.

The remainder of this article is organized as follows. The dynamic model of the vehicle with RACS is formulated in the following section. In Section 3, the lateral dynamic behavior of the vehicle with RACS is demonstrated. In Section 4, shimmy factors of the compliance steering wheel are investigated. Finally, in the last section, concluding remarks are provided.

2. Dynamic Model of Vehicle with RACS

In this section, dynamic model of the vehicle with RACS is studied. A kind of viscoelastic material is introduced into the rear suspension. First of all, a fractional order model of RACS incorporating viscoelastic material is proposed, and then, the nonlinear dynamic model of the vehicle with RACS is formulated.

2.1. Fractional Order Model of RACS. Based on the assumptions applied to the well-known bicycle model, the yaw-plane model of the vehicle with RACS can be obtained. Assuming that the RACS system is disassembled from the vehicle body (the rear wheel and the force F_r are drawn with dotted line), the lateral forces on the vehicle applied by the RACS system can be shown in Figure 1(a). Figure 1(b) shows the RACS system and the corresponding position for points O_2, O_3, and Q. In this study, torsion beam suspension in Figure 1(b) is chosen as the most suitable suspension for actualizing compliance steering of the rear wheels.

Viscoelastic models containing fractional derivative of different orders and other fractional operators with more than one independent fractional parameter have long attracted the attention of investigators. The typical models are listed as equations (1) and (2) [13]. Equation (1a) is the fractional derivative Maxwell model with two independent fractional parameters. Palade et al. [14] have shown that model (1a) could be used to describe the entire viscoelastic behavior of polybutadiene from flow to glassy regime:

$$\sigma + \tau_\varepsilon^\alpha D^\alpha \sigma = E_\infty \tau_\varepsilon^\gamma D^\gamma \varepsilon. \tag{1a}$$

The modified fractional derivative Maxwell model is written as follows:

$$\sigma + \tau_\varepsilon^\alpha D^\alpha \sigma = E_\infty \left(\tau_\varepsilon^\alpha D^\alpha \varepsilon + \tau_\varepsilon^\gamma D^\gamma \varepsilon\right). \tag{1b}$$

Another model of frequent use is the generalized standard linear solid model with two independent fractional parameters, which is expressed as equation (2a) or (2b) which has one additional term in the right-hand side of equation (2a) [15]:

$$\sigma + \tau_\varepsilon^\alpha D^\alpha \sigma = E_0 \left(\varepsilon + \tau_\sigma^\gamma D^\gamma \varepsilon\right), \tag{2a}$$

$$\sigma + \tau_\varepsilon^\alpha D^\alpha \sigma = E_0 \left(\varepsilon + \tau_\sigma^\alpha D^\alpha \varepsilon + \tau_\sigma^\gamma D^\gamma \varepsilon\right). \tag{2b}$$

Some research results have demonstrated the excellent agreement between the five-parametric model (3) and the mechanical properties of the viscoelastic material [16, 17]. Therefore, equation (2a) is adopted to describe the constitutive relation of the viscoelastic material in this study.

In the above equations, parameters α and γ ($0 < \alpha$ and $\gamma \le 1$) are fractional parameters, and $D^\alpha(\cdot)$ and $D^\gamma(\cdot)$ represent Riemann–Liouville fractional derivatives of the order α and γ, respectively, which are defined as follows [18]:

$$D^\xi x = \frac{1}{\Gamma(1-\xi)} \frac{d}{dt} \int_0^t \frac{x(\tau)}{(t-\tau)^\xi} d\tau \, (0 < \xi < 1), \tag{3}$$

where ξ is the fractional order of the time derivative, D^ξ represents the operator of fractional derivation of ξth order, and Γ denotes the Euler gamma function [19].

When rear wheel produces a compliance steering angle δ_c, the viscoelastic unit will deform and cause axial elastic force F_d. Assuming that the viscoelastic unit is homogeneous, its cross-sectional area is A and its axial length is h. Then, equation (4) can be obtained as follows:

$$F_d + \tau_\varepsilon^\alpha D^\alpha F_d = A E_0 \left(\varepsilon + \tau_\sigma^\gamma D^\gamma \varepsilon\right). \tag{4}$$

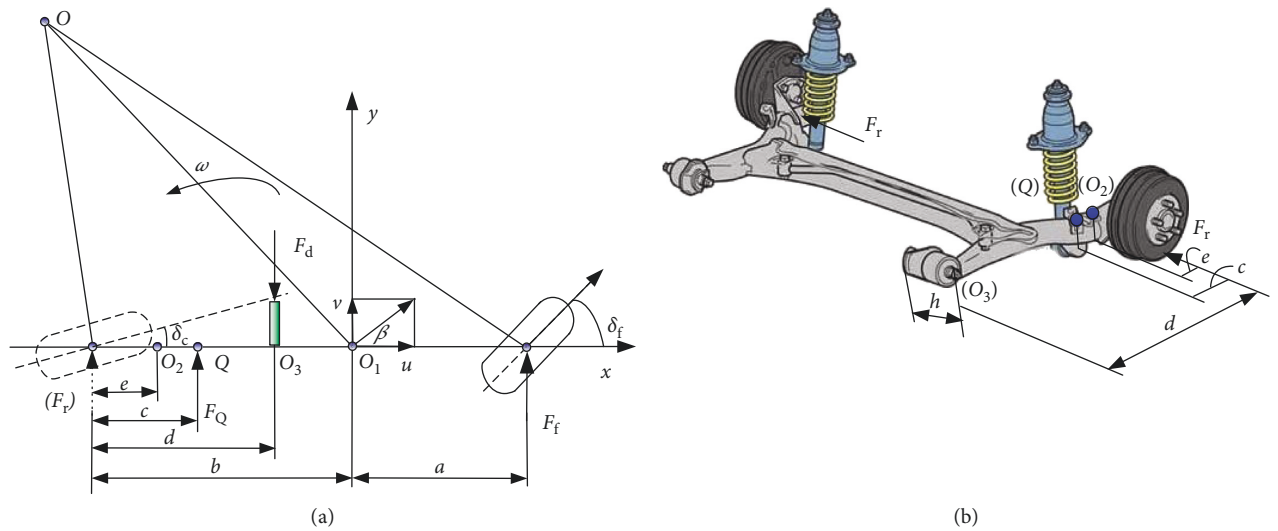

Figure 1: Schematic diagram for vehicle with RACS.

According to the definition of strain, equation (4) can be further expressed as follows:

$$F_{\mathrm{d}}\left(1+\tau_{\varepsilon}^{\alpha}D^{\alpha}\right)=C_{\mathrm{s}}\delta_{\mathrm{c}}\left(1+\tau_{\sigma}^{\gamma}D^{\gamma}\right), \tag{5}$$

where C_{s} is the stiffness of RACS system, which is given in the following equation:

$$C_{\mathrm{s}}=\frac{dAE_0}{h}. \tag{6}$$

2.2. Dynamic Model of Vehicle. When the front wheel turns at angle δ_{f}, the rear wheel produces the compliance steering angle δ_{c}. Assuming the sideslip angle β is small and $|\beta|\ll 1$, the sideslip angles of front and rear wheels can be written as follows:

$$\begin{cases}\alpha_{\mathrm{f}}=\beta+\dfrac{a\omega}{u}-\delta_{\mathrm{f}},\\[2ex]\alpha_{\mathrm{r}}=\beta-\dfrac{b\omega}{u}-\delta_{\mathrm{c}}.\end{cases} \tag{7}$$

The Magic formula tire model is widely used for its high precision in describing tire properties [20]. In this study, the magic formula tire model is adopted, as given in the following equation:

$$y'=D\sin\left\{C\arctan\left\{B(1-E)\left(x'+S_{\mathrm{h}}\right)+E\arctan\left(B\left(x'+S_{\mathrm{h}}\right)\right)\right\}\right\}+S_{\mathrm{v}}, \tag{8}$$

where y' denotes the output variable, which is the tire longitudinal force or lateral force; x' denotes the input variable, which is the tire longitudinal slip ratio or sideslip angle; B is the tire stiffness factor; C is the tire shape factor; D is the tire peak factor; E is the tire curvature factor; S_{h} and S_{v} represent origin offset of coordinates when considering original sideslip angle of the tire. Tire parameters listed in Table 1 are obtained through fitting the experimental data in the literature [21]. The cornering characteristics of tires for front and rear wheels are shown in Figure 2.

Table 1: Parameters of magic formula tire model.

Parameters	B	C	D	E
Front wheel	6.64	1.352	−5822	−1.999
Rear wheel	8.76	1.352	−5920	−1.7098

We assume that the longitudinal velocity u is a constant, RACS is an equivalent linear model, and the geometrical nonlinearity of the vehicle is ignored. According to Newton's second law, dynamical equation of vehicle with RACS can be expressed as follows:

$$\begin{cases}(m+m_{\mathrm{c}})\dot{v}-(b-e)m_{\mathrm{c}}\dot{\omega}+em_{\mathrm{c}}\ddot{\delta}_{\mathrm{c}}=-mu\omega+F_{\mathrm{f}}+F_{\mathrm{r}},\\(b-c)m_{\mathrm{c}}\dot{v}-\left[(b-e)(b-c)m_{\mathrm{c}}+I_{\mathrm{Z}}\right]\dot{\omega}+e(b-c)m_{\mathrm{c}}\ddot{\delta}_{\mathrm{c}}\\\quad=-aF_{\mathrm{f}}+(b-c)F_{\mathrm{r}}+(d-c)F_{\mathrm{d}},\\(c-e)m_{\mathrm{c}}\dot{v}-\left[(c-e)(b-e)m_{\mathrm{c}}+I_{\mathrm{cs}}\right]\dot{\omega}\\\quad+\left[e(c-e)m_{\mathrm{c}}-I_{\mathrm{cs}}\right]\ddot{\delta}_{\mathrm{c}}=cF_{\mathrm{r}}-(d-c)F_{\mathrm{d}}.\end{cases} \tag{9}$$

Taking the lateral velocity v and the yaw rate ω as state variables, equation (9) can be transformed into state space form, as given in equations (10) and (11):

$$E_1\begin{bmatrix}\dot{v}\\\dot{\omega}\end{bmatrix}=A_1\begin{bmatrix}v\\\omega\end{bmatrix}+B_1\begin{bmatrix}F_{\mathrm{f}}\\F_{\mathrm{r}}\\F_{\mathrm{d}}\end{bmatrix}, \tag{10}$$

$$\ddot{\delta}_{\mathrm{c}}=A_2\begin{bmatrix}\dot{v}\\\dot{\omega}\end{bmatrix}+B_2\begin{bmatrix}F_{\mathrm{f}}\\F_{\mathrm{r}}\\F_{\mathrm{d}}\end{bmatrix}, \tag{11}$$

where matrices E_1, A_1, B_1, and B_2 are defined as follows:

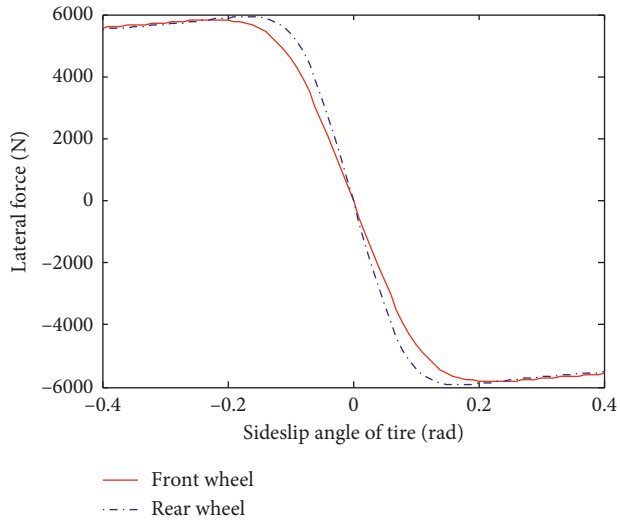

Figure 2: Cornering characteristics of tires.

$$E_1 = \begin{bmatrix} \dfrac{(c-e)m_c}{e(c-e)m_c - I_{cs}} - \dfrac{(m+m_c)}{em_c} & \dfrac{(b-e)m_c}{em_c} - \dfrac{(b-e)(c-e)m_c + I_{cs}}{e(c-e)m_c - I_{cs}} \\ \dfrac{(c-e)m_c}{e(c-e)m_c - I_{cs}} - \dfrac{1}{e} & \dfrac{(b-e)(b-c)m_c + I_Z}{e(b-c)m_c} - \dfrac{(c-e)(b-e)m_c + I_{cs}}{e(c-e)m_c - I_{cs}} \end{bmatrix},$$

$$A_1 = \begin{bmatrix} 0 & \dfrac{mu}{em_c} \\ 0 & 0 \end{bmatrix},$$

$$A_2 = \begin{bmatrix} -\dfrac{em_c}{e(c-e)m_c - I_{cs}} & \dfrac{e(b-c+e)m_c + I_{cs}}{e(c-e)m_c - I_{cs}} \end{bmatrix}, \tag{12}$$

$$B_1 = \begin{bmatrix} -\dfrac{1}{em_c} & \dfrac{c}{e(c-e)m_c - I_{cs}} - \dfrac{1}{em_c} & -\dfrac{d-c}{e(c-e)m_c - I_{cs}} \\ \dfrac{a}{e(b-c)m_c} & \dfrac{c}{e(c-e)m_c - I_{cs}} - \dfrac{b-c}{e(b-c)m_c} & \dfrac{c-d}{e(c-e)m_c - I_{cs}} - \dfrac{d-c}{e(b-c)m_c} \end{bmatrix},$$

$$B_2 = \begin{bmatrix} 0 & \dfrac{c}{e(c-e)m_c - I_{cs}} & -\dfrac{d-c}{e(c-e)m_c - I_{cs}} \end{bmatrix}.$$

3. Demonstration of Lateral Dynamic Behavior

In this section, numerical demonstration of lateral dynamic behavior for the vehicle with RACS is carried out in MATLAB, and some nonlinear dynamical phenomena are also analyzed.

Parameter values for the baseline vehicle are as follows: $m = 1740$ kg, $I_z = 3048$ kg m^2, $a = 1.46$ m, and $b = 1.54$ m. Preliminary values of relevant parameters for the RACS system are listed as follows: $m_c = 100$ kg, $I_{cs} = 100$ kg·m^2, $e = 0.15$ m, $d = 0.8$ m, and $c = 0.35$ m. And the parameter values for the viscoelastic material are preliminarily chosen as follows: $\tau_\varepsilon = \tau_\sigma = 1$, $E_0 = 0.5 \times 10^5$ MPa, $\alpha = 0.3$, and $\gamma = 0.7$. Based on the above parameter values and the steering angle input of the front wheel $\delta_f = 0.01$ rad, numerical demonstrations for the vehicle with RACS are performed.

The relationship between compliance steering angle δ_c and vehicle longitudinal velocity u is shown in Figure 3. It can be seen that a bifurcation occurs when the velocity u exceeds the critical velocity 10.2 m/s. Bifurcation in a shimmy analysis is frequently called Hopf bifurcation, which creates limit cycles from an equilibrium point as a bifurcation parameter crosses a critical value [22]. Hopf bifurcation is a local bifurcation in which a fixed point of the dynamical system loses stability [23]. In Figure 3, Hopf bifurcation of the compliance steering angle leads to the shimmy of the compliance steering

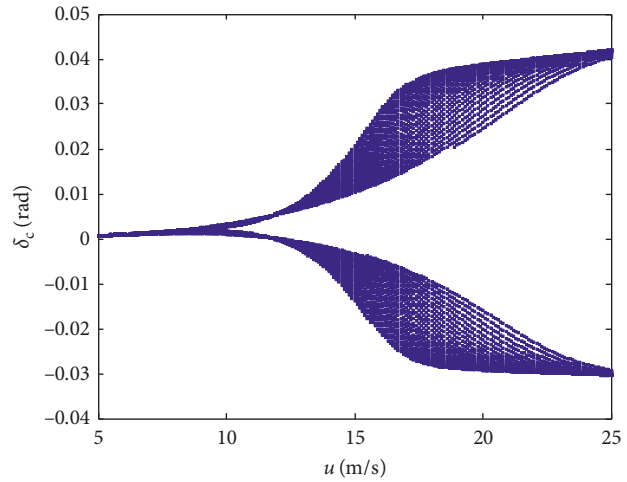

Figure 3: Relationship between compliance steering angle δ_c and the velocity u.

wheel. Hopf bifurcation is supercritical at the critical velocity 10.2 m/s. When the velocity is smaller than 10.2 m/s, shimmy does not occur in the compliance steering wheel; when the velocity is larger than 10.2 m/s, shimmy occurs. Therefore, the compliance steering wheel shimmy is a typical self-excited vibration. With the velocity increasing, the self-excited oscillation amplitude of the compliance steering angle increases.

For longitudinal velocity $u = 10$ m/s, Figure 4 shows the time history of compliance steering angle and yaw rate, respectively. Figure 4(a) mentions that the oscillation amplitude of the compliance steering angle for the rear wheel is a little large at the beginning of oscillation, and it takes about seven seconds to reach its steady-state value. Figure 4(b) shows that the yaw rate of the vehicle behaves with similar performance as that of the compliance steering angle. As the vehicle velocity is smaller than the critical velocity of shimmy, compliance steering angle and yaw rate of the vehicle are both able to reach the stable state after a period of attenuation oscillation.

For longitudinal velocity $u = 20$ m/s, Figure 5 shows the time history of compliance steering angle and yaw rate, respectively. It can be seen that the curves present obvious fluctuation phenomena, which is also in accordance with the conclusion shown in Figure 3. If the velocity is larger than the critical velocity of shimmy, the vehicle will experience a shimmy phenomenon.

Figure 6 shows the phase diagram of compliance steering angle for $u = 10$ m/s and $u = 20$ m/s, respectively. In Figure 6, the horizontal axis is the compliance steering angle δ_c and the vertical axis is the compliance steering angular velocity $\dot{\delta}_c$. Figure 6(a) shows that when the velocity is smaller than the critical velocity of shimmy, the vehicle is stable and the equilibrium point is a stable focus. At the equilibrium point, the compliance steering angular velocity tends to zero and the compliance steering angle tends to a constant value. In Figure 6(b), when the velocity is larger than the critical velocity of shimmy, the equilibrium point is an unstable focus and there appear limit cycles in the phase diagram. The occurrence of limit cycles means that dynamical equation of the vehicle with RACS has periodic solutions and periodic oscillations occur in the vehicle.

4. Analyses of Shimmy Factors

Many factors contribute to vehicle shimmy phenomenon, such as dynamic balance, stiffness, damping, working clearance, dry friction, wheel alignment parameters, and motion interference [24]. Currently, studies on wheel shimmy are carried out mostly aiming at the front wheel shimmy [25]. However, for the vehicle with RACS, the compliance steering wheel shimmy is very important for vehicle stability. In this section, shimmy factors of the compliance steering wheel are discussed from the following three aspects.

4.1. Effects of Viscoelastic Material Properties on Shimmy. Parameters of the viscoelastic material used in rear suspension have important effect on the vehicle shimmy phenomenon. In this study, constitutive relation of the viscoelastic material is described through five material parameters (σ, ε, τ_ε, τ_σ, and E_0) and two fractional parameters (α and γ), as mentioned in subsection 2.1. The five material parameters and the two fractional parameters may all have an impact on the vehicle shimmy. In the present study, the influence of fractional order α and elastic modulus E_0 on vehicle shimmy is discussed through numerical experiments.

In the numerical cases, the vehicle velocity u is set as 20 m/s and the fractional order α is set as 0.3, 0.4, and 0.5, respectively. Other parameters of the vehicle and viscoelastic material are given in Section 2. Figure 7 shows the effect of the fractional order α on the compliance steering angle δ_c and the yaw rate γ for the case of $E_0 = 0.5 \times 10^5$ MPa. It can be observed that α has obvious effect on the compliance steering angle and the yaw rate. The compliance steering angle and the yaw rate occur periodic fluctuation with a higher level when the fractional order $\alpha = 0.5$; the amplitude of periodic fluctuation decreases obviously when the fractional order $\alpha = 0.4$; and the periodic fluctuation disappears and the vehicle becomes stable when the fractional order $\alpha = 0.3$. Furthermore, the smaller the order α is, the closer to zero the amplitude of periodic fluctuation is. Obviously, by changing the fractional order α of the viscoelastic material can control shimmy of the vehicle with RACS.

In the next numerical cases, the effects of the elastic modulus E_0 on the dynamic behavior of the vehicle with RACS are investigated. The elastic modulus is set as $E_0 = 0.8 \times 10^5$ MPa, u is set as 20 m/s and α is set as 0.3, 0.4, and 0.5, respectively. Other parameters are not changed. Figure 8 shows the effect of the fractional order α on the compliance steering angle δ_c and the yaw rate γ for the case of $E_0 = 0.8 \times 10^5$ MPa. Compared with Figure 7, it can be seen that with increasing of elastic modulus E_0, the stability of compliance steering angle and yaw rate are both obviously improved. Even, the shimmy phenomenon of the vehicle is improved when the fractional order $\alpha = 0.5$. In evidence, raising the elastic modulus E_0 of the viscoelastic material contributes to the lateral stability of the vehicle with RACS.

4.2. Effects of RACS Parameters on Shimmy. In this subsection, the effects of RACS dimension parameter c and mass

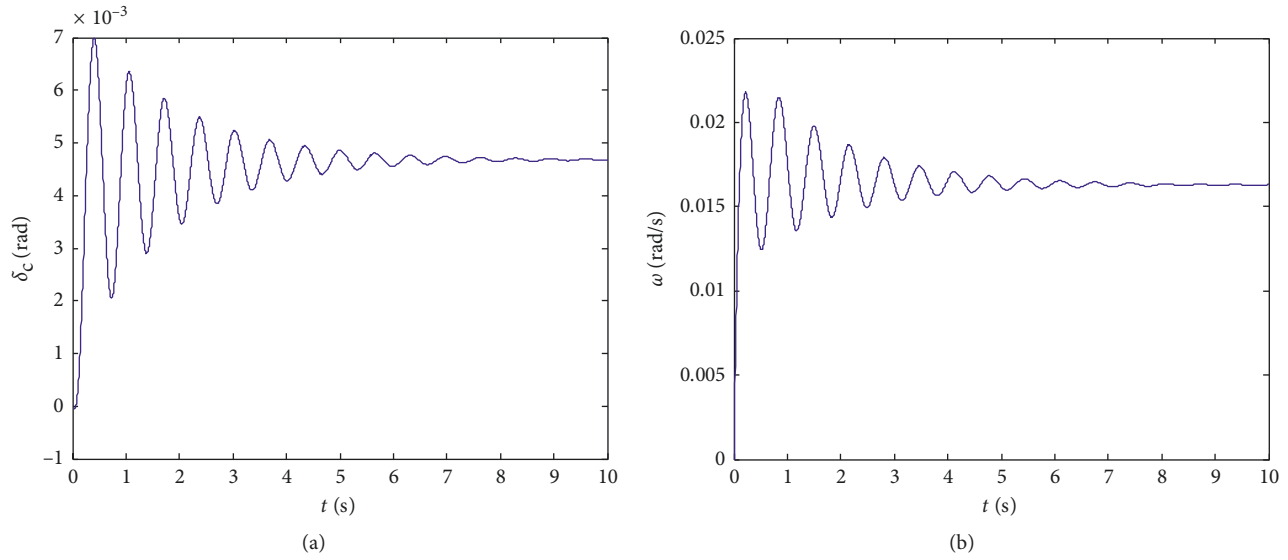

Figure 4: Time history of (a) compliance steering angle and (b) yaw rate, for the case of $u = 10$ m/s.

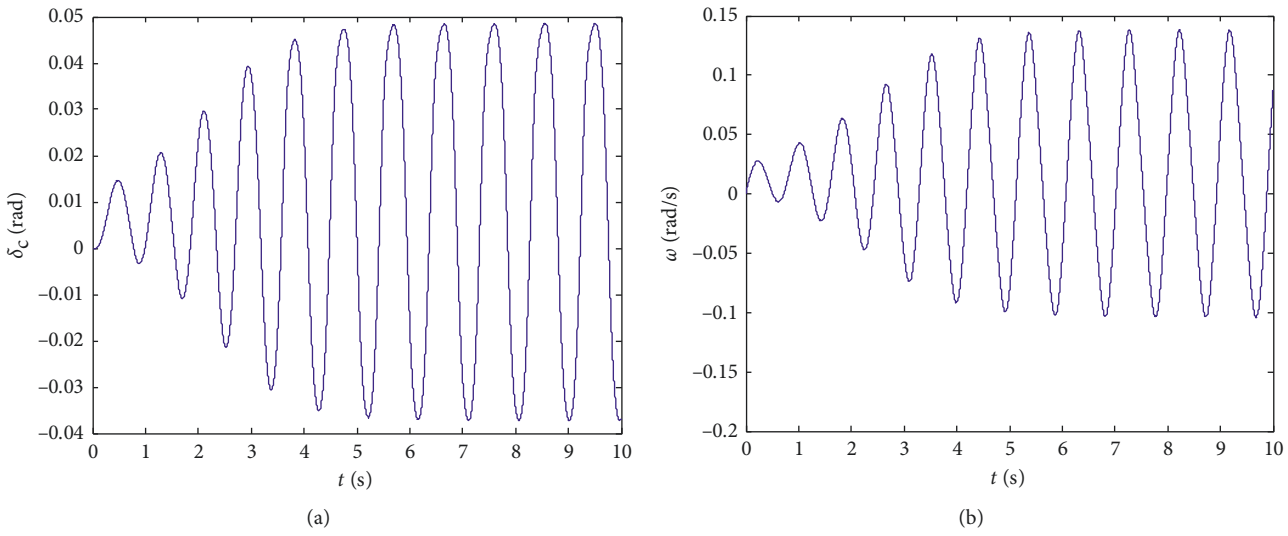

Figure 5: Time history of (a) compliance steering angle and (b) yaw rate, for the case of $u = 20$ m/s.

parameter m_c on vehicle shimmy are investigated. The parameter c is the distance between the rear axle center and the main axle of rear suspension, m_c is the mass of the RACS system.

Figure 9 shows the effects of parameter c on the compliance steering angle when u is set as 20 m/s and m_c equals to 100 kg. It can be seen that when c is a small value, the compliance steering angle is in a stable state. When c increases to 0.15 m, Hopf bifurcation of the compliance steering angle occurs, which leads to the shimmy of the compliance steering wheel. With the further increase of c, the vehicle with RACS runs into serious unstable state, which is a chaos state. Figure 10 demonstrates the effects of parameter m_c on the compliance steering angle when c equals to different values. It is obvious that the larger the value of c is, the greater the oscillation degree of the rear wheel is. Figure 11 shows the phase diagrams of the compliance steering angle of the rear wheel when c equals to 0.2 and 0.3, which respectively correspond to the periodic motion and chaotic motion of the rear wheel. As can be seen from above analyses, the dimension parameter c has a significant influence on vehicle shimmy, and it should be reasonably designed.

From Figure 10(a), it can be seen that, when the mass m_c is less than 160 kg, the vehicle is in an unstable oscillating state, and the compliance steering angle δ_c changes asymmetrically. The smaller the mass is, the greater the oscillation degree is. When the mass m_c is larger than 160 kg, the vehicle enters a relatively steady state. Figure 12 shows the phase diagram of the compliance steering angle of the rear wheel when m_c equals to 30 kg, which corresponds to the periodic motion of the rear wheel.

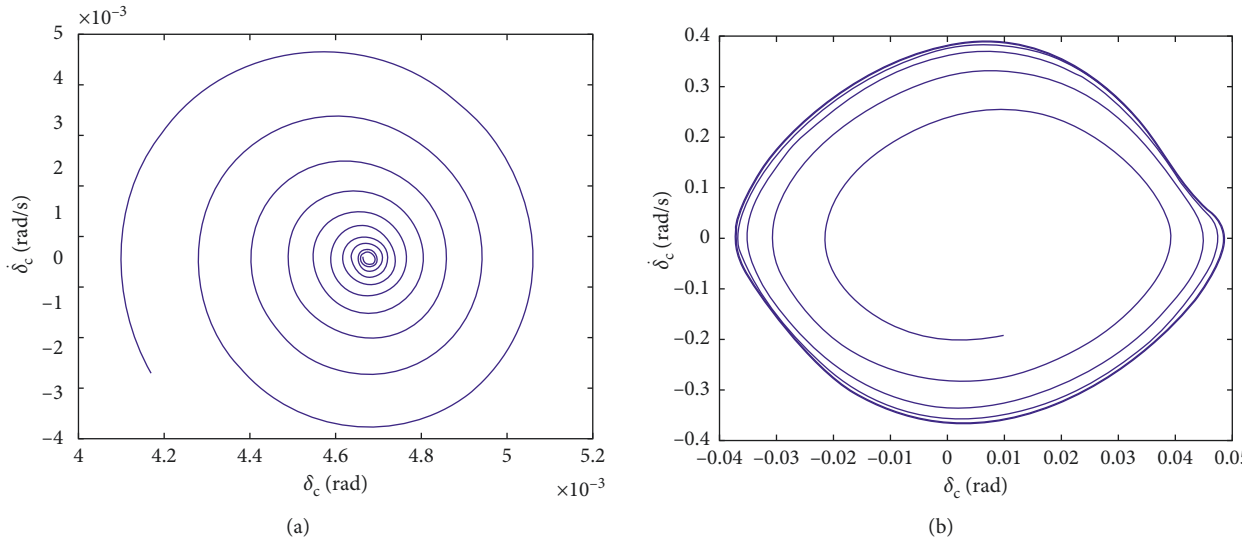

Figure 6: Phase diagram of compliance steering angle: (a) $u = 10$ m/s and (b) $u = 20$ m/s.

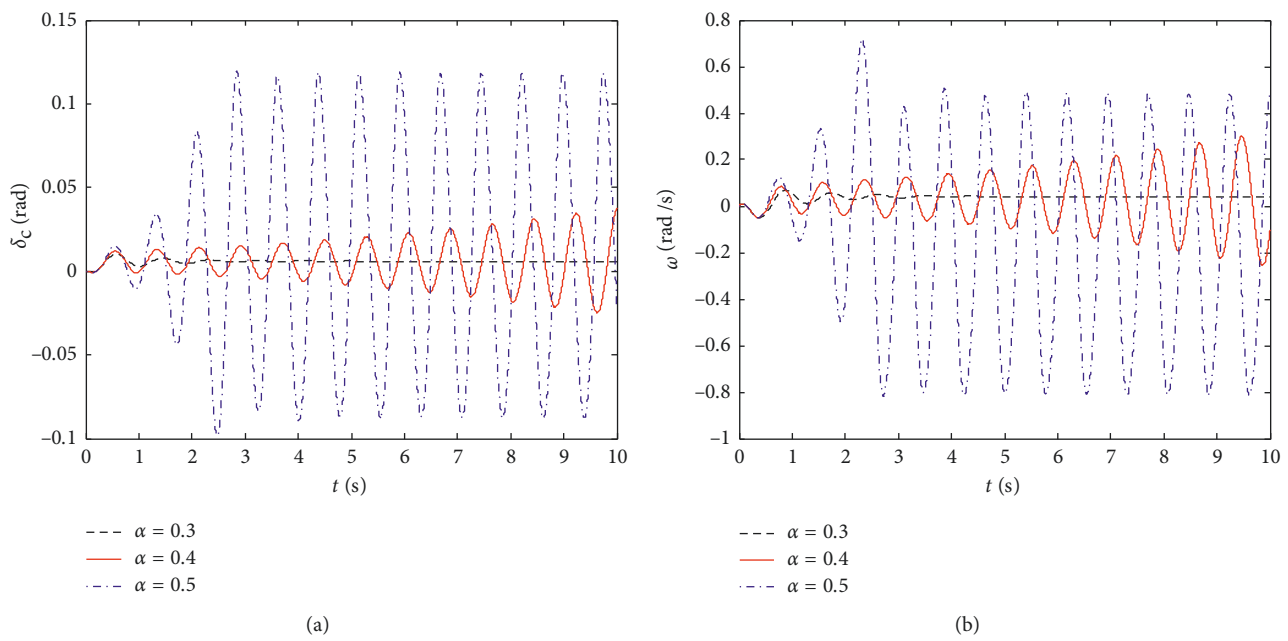

Figure 7: Effects of α on (a) compliance steering angle and (b) yaw rate, for the case of $E_0 = 0.5 \times 10^5$ MPa.

4.3. Effects of Front Wheel Steering Angle on Shimmy. The swing vibration of the rear wheel belongs to self-excited vibration, and under certain conditions, the steering angle of the front wheel may become the initial excitation for whole nonlinear vehicle model. In this subsection, the effect of the front wheel steering angle on vehicle shimmy is investigated.

Figure 13 shows the effect of the front wheel steering angle δ_f on the compliance steering angle δ_c when u is set as 20 m/s. In the figure, when the front wheel steering angle is smaller than 0.08 rad, periodic oscillation of the compliance steering angle occurs and when the front wheel steering angle is larger than 0.08 rad, the compliance steering angle maintains a stable value, which means the vehicle is in a stable state. Figure 14 shows the phase diagrams of the compliance steering angle of the rear wheel when δ_f equals to 0.04 and 0.12. When δ_f equals to 0.04, periodic motion of the rear wheel occurs. When δ_f equals to 0.12, the vehicle is stable and the equilibrium point is a stable focus. The results are consistent with the dynamic response of the actual vehicle. Larger front wheel steering angle means the vehicle is running on the curve road, and under this condition, the shimmy of the compliance steering wheel is inhibited by the tire lateral force. However, when the front wheel steering angle is a smaller value, which means the vehicle is running on an approximate straight-line road, the periodical vibration with a smaller amplitude occurs in the compliance steering wheel.

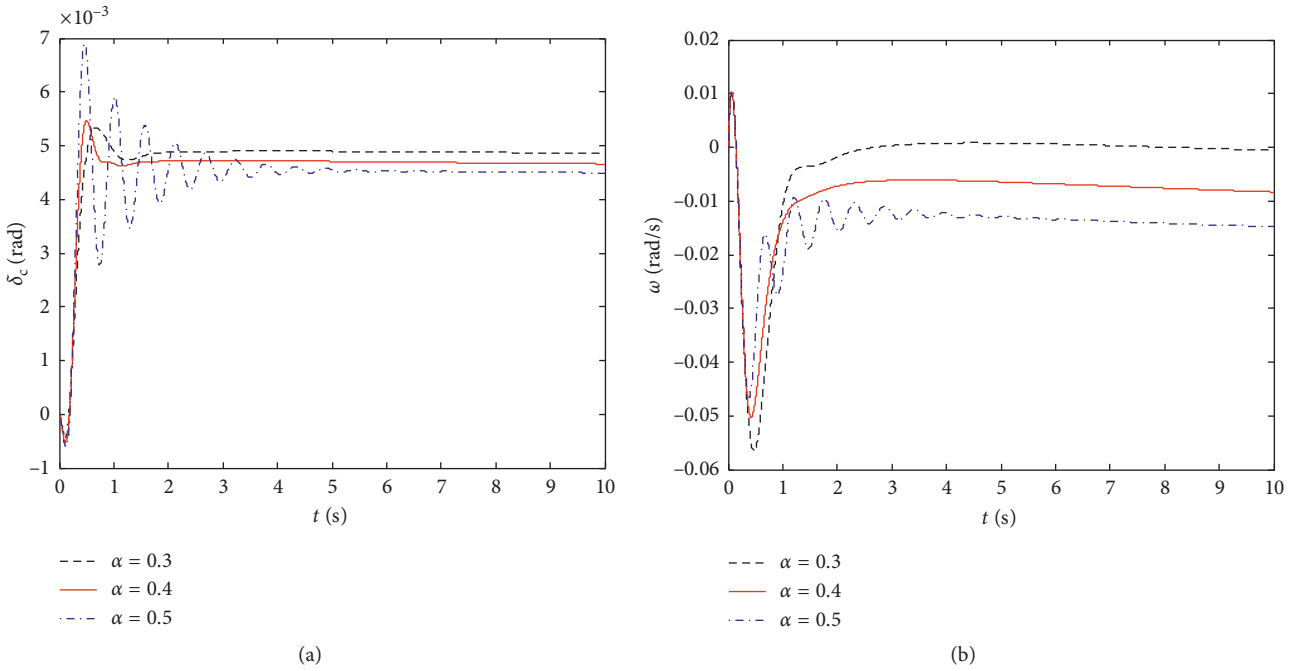

Figure 8: Effects of α on (a) compliance steering angle and (b) yaw rate, for the case of $E_0 = 0.8 \times 10^5$ MPa.

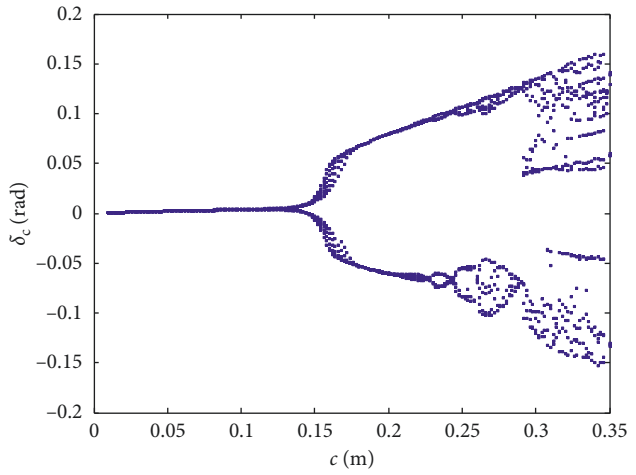

Figure 9: Effects of c on the compliance steering angle δ_c.

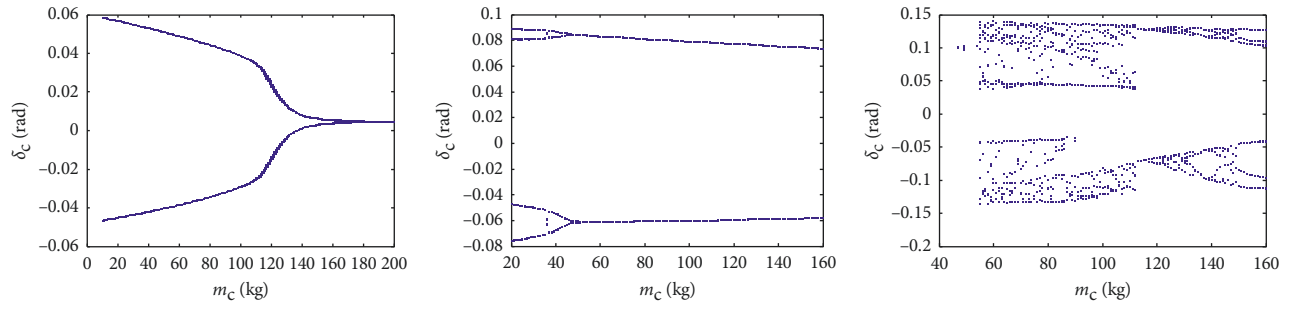

Figure 10: Effects of m_c on the compliance steering angle δ_c: (a) $c = 0.15$, (b) $c = 0.2$, and (c) $c = 0.3$.

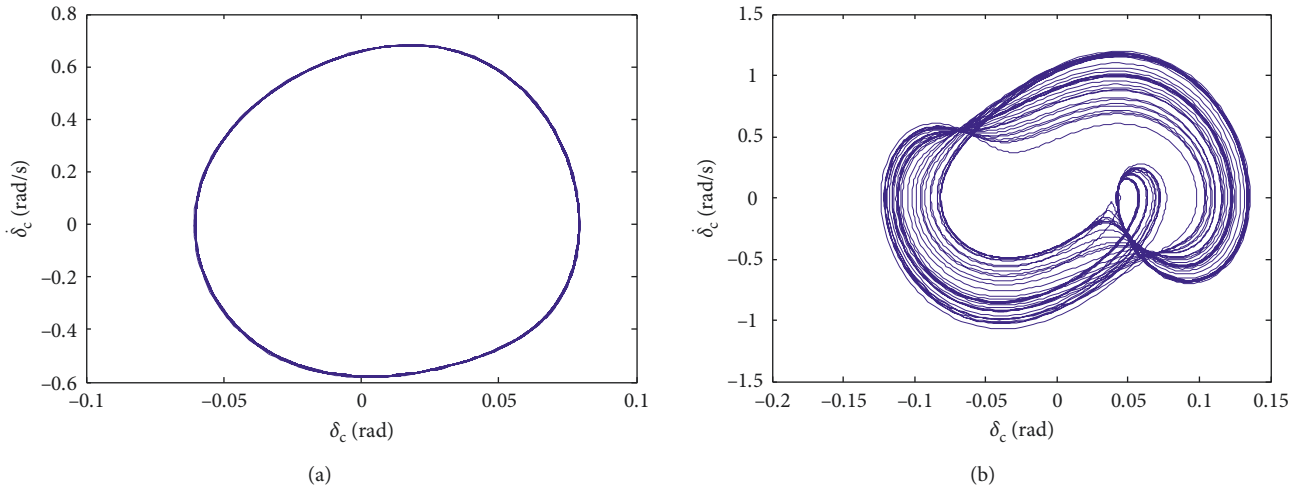

Figure 11: Phase diagrams of the compliance steering angle: (a) $c = 0.2$, $m_c = 100$ kg and (b) $c = 0.3$, $m_c = 100$ kg.

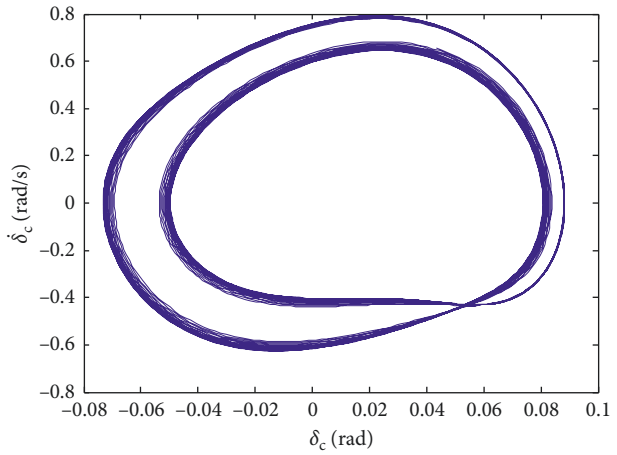

Figure 12: Phase diagram of the compliance steering angle when $m_c = 30$ kg and $c = 0.2$.

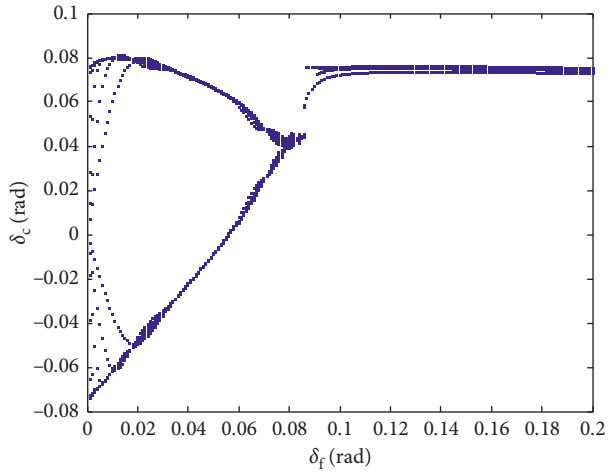

Figure 13: Effects of δ_f on the compliance steering angle δ_c.

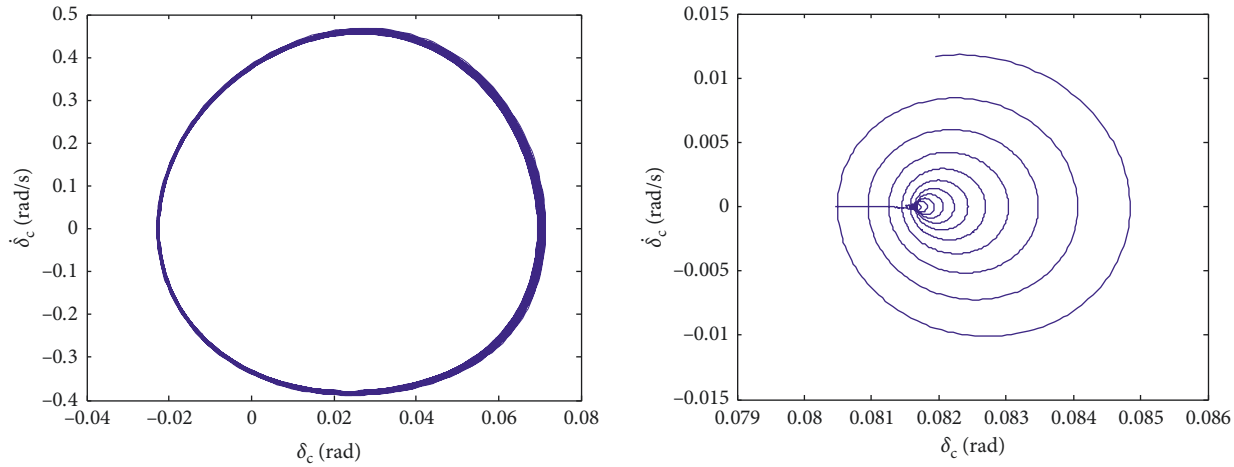

Figure 14: Phase diagrams of the compliance steering angle: (a) $\delta_f = 0.04$ and (b) $\delta_f = 0.12$.

5. Conclusions

A kind of viscoelastic smart material, whose properties can be depicted by fractional derivative constitutive relation, is introduced into the rear suspension of a vehicle to construct a rear wheel semiactive steering system. Considering the tire nonlinearity, the nonlinear dynamic model of the vehicle with RACS is formulated. The nonlinear dynamic behavior of the vehicle is demonstrated, and its influence factors are investigated through numerical experiments. Some findings can be summarized as follows:

(1) For the vehicle with RACS, under certain parameter conditions when the longitudinal velocity is larger than the critical velocity, shimmy phenomenon occurs in the compliance steering wheel. The shimmy of the compliance steering wheel is a typical self-excited vibration. The longitudinal velocity is an important bifurcation parameter in the wheel shimmy. With the longitudinal velocity increasing, the amplitude of the self-excited oscillation increases.

(2) The fractional order used to depict the constitutive relation of the viscoelastic material has obvious effect on the compliance steering angle and the yaw rate of the vehicle. When the fractional order takes a larger value, compliance steering angle and the yaw rate occur periodic fluctuation with a higher level. When the fractional order takes a smaller value, the periodic fluctuation disappears and the vehicle becomes stable. Therefore, it can be concluded that by changing the fractional order of the viscoelastic material incorporated in RACS can control shimmy of the vehicle with RACS.

(3) The elastic modulus of the viscoelastic material incorporated in RACS has obvious effect on the compliance steering angle and the yaw rate of the vehicle. Raising the elastic modulus contributes to the lateral stability of the vehicle with RACS.

(4) The dimension parameter of RACS, distance between the rear axle center and the main axle of rear suspension, has a significant influence on vehicle shimmy. When the parameter value is larger than its critical value, the vehicle shimmy occurs. The larger the parameter value is, the more serious the vehicle shimmy becomes. So, it is very important to design this parameter reasonably. The mass of RACS also influences the shimmy phenomenon of the vehicle with RACS to some extent. The larger mass value of RACS contributes to the lateral stability of the vehicle with RACS.

(5) The front wheel steering angle has a certain impact on the shimmy of the vehicle with RACS. The smaller front wheel steering angle will lead to periodic motion of the compliance steering wheel.

Nomenclature

O: Instantaneous center of vehicle rotation
O_1: Center of gravity (CG) of the vehicle
O_2: Center of gravity (CG) of the RACS system
O_3: Position of the axial elastic force caused by viscoelastic material deforming
Q: Position of the main axle of rear suspension
a: Distance between the vehicle CG and the front axle center of the vehicle
b: Distance between the vehicle CG and the rear axle center of the vehicle
c: Distance between the rear axle center and the main axle of rear suspension
d: Distance between the rear axle center and the axis of viscoelastic unit
e: Distance between the rear axle center and the CG of the RACS system
h: Axial length of the viscoelastic material
δ_f: Steering angle of the front wheel
δ_c: Compliance steering angle of the rear wheel

$\ddot{\delta}$: Angular acceleration of the compliance steering for the rear wheel
β: Sideslip angle β at the vehicle CG
u: Longitudinal velocity at the vehicle CG
v: Lateral velocity at the vehicle CG
$\dot{v}$: Lateral acceleration at the vehicle CG
ω: Yaw rate of the vehicle
$\dot{\omega}$: Angular acceleration of the vehicle yaw motion
F_f: Lateral force on the front wheel applied by the ground
F_r: Lateral force on the rear wheel applied by the ground
F_Q: Lateral force on the vehicle body applied by the main axle of rear suspension
F_d: Axial elastic force on the vehicle body caused by viscoelastic material deforming
σ: Stress of the viscoelastic material
ε: Strain of the viscoelastic material
τ_ε: Relaxation time of the viscoelastic material
τ_σ: Creep time of the viscoelastic material
E_0: Relaxed magnitude of elastic modulus
m: Mass of the vehicle
m_c: Mass of the RACS system
I_z: Inertia moment of the vehicle about the yaw axis
I_{cs}: Inertia moment of the RACS system about the yaw axis.

Data Availability

The data used to support the findings of this study are available from the corresponding author upon request.

Conflicts of Interest

The authors declare that there are no conflicts of interest regarding the publication of this paper.

Acknowledgments

This work is supported by National Natural Science Foundation of China (Grant nos. 51605228 and 11272159), Project of Talent Peak Covering Six Industries in Jiangsu Province (Grant no. JXQC-025), and Youth Science & Technology Innovation Project of Nanjing Forestry University (Grant no. CX2016028).

References

[1] Y. Furukawa, N. Yuhara, S. Sano, H. Takeda, and Y. Matsushita, "A review of four-wheel steering studies from the viewpoint of vehicle dynamics and control," *Vehicle System Dynamics*, vol. 18, no. 1–3, pp. 151–186, 2007.

[2] M. Kreutz, M. Horn, and J. Zehetner, "Improving vehicle dynamics by active rear wheel steering systems," *Vehicle System Dynamics*, vol. 47, no. 12, pp. 1551–1564, 2009.

[3] X. M. Xu, N. Chen, and H. P. Lee, "A review on the applied research of rear wheel compliance steering," *Automobile Technology*, vol. 7, pp. 1–6, 2016, in Chinese.

[4] F. Momiyama and K. Miyazaki, "Compliance steer and road holding of rigid rear axle for enhancing the running straightness of large sized vehicles," in *Proceedings of International Truck & Bus Meeting & Exposition*, Detroit, MI, USA, November 1993.

[5] B. Piquet, C. A. Mass, and F. Capou, "Next generation of suspension bushings: review of current technologies and expansion upon new 3rd generation product data," in *Proceedings of SAE Technical Paper*, Detroit, MI, USA, April 2007.

[6] R. N. Yerrawar and R. R. Arakerimath, "Development of methodology for semi active suspension system using MR damper," *Materials Today: Proceedings*, vol. 4, no. 8, pp. 9294–9303, 2017.

[7] X. M. Xu, Y. P. Jiang, N. Chen, and H. P. Lee, "Dynamic behavior of a vehicle with rear axle compliance steering," *Journal of Vibroengineering*, vol. 19, no. 6, pp. 4483–4497, 2017.

[8] J. Lu, J. Jiang, J. Li, and M. Wen, "Analysis of dynamic mechanism and global response of vehicle shimmy system with multi-clearance joints," *Journal of Vibration and Control*, vol. 24, no. 11, pp. 2312–2326, 2016.

[9] S. Ran, I. J. M. Besselink, and H. Nijmeijer, "Application of nonlinear tyre models to analyse shimmy," *Vehicle System Dynamics*, vol. 52, no. 1, pp. 387–404, 2014.

[10] S. Dutta and S.-B. Choi, "Control of a shimmy vibration in vehicle steering system using a magneto-rheological damper," *Journal of Vibration and Control*, vol. 24, no. 4, pp. 797–807, 2016.

[11] T. Mi, G. Stepan, D. Takacs, N. Chen, and N. Zhang, "Model establishment and parameter analysis on shimmy of electric vehicle with independent suspensions," *Procedia IUTAM*, vol. 22, pp. 259–266, 2017.

[12] L. B. Eldred, W. P. Baker, and A. N. Palazotto, "Kelvin-Voigt versus fractional derivative model as constitutive relations for viscoelastic materials," *AIAA Journal*, vol. 33, no. 3, pp. 547–550, 2012.

[13] Y. A. Rossikhin and M. V. Shitikova, "Analysis of rheological equations involving more than one fractional parameters by the use of the simplest mechanical systems based on these equations," *Mechanics of Time-Dependent Materials*, vol. 5, no. 2, pp. 131–175, 2001.

[14] L.-I. Palade, V. Verney, and P. Attan, "A modified fractional model to describe the entire viscoelastic behavior of polybutadienes from flow to glassy regime," *Rheologica Acta*, vol. 35, no. 3, pp. 265–273, 1996.

[15] C. Friedrich, "Relaxation functions of rheological constitutive equations with fractional derivatives: thermo-dynamical constraints," in *Lecture Notes in Physics*, pp. 321–330, Springer, Berlin, Germany, 1991.

[16] P. Cupial, "Some approaches to the analysis of non-proportionally damped viscoelastic structures," in *Proceedings of International Symposium on Dynamics of Continua*, pp. 93–102, Berlin, Germany, January 1996.

[17] D. R. Morgenthaler, "Practical design and analysis of systems with fractional derivative materials and active control," in *Proceedings of Damping'91*, vol. 1, pp. 1–28, San Diego, CA, USA, February 1991.

[18] V. Lakshmikantham and A. S. Vatsala, "Basic theory of fractional differential equations," *Nonlinear Analysis: Theory, Methods & Applications*, vol. 69, no. 8, pp. 2677–2682, 2008.

[19] B. Ross, "A brief history and exposition of the fundamental theory of fractional calculus," *Lecture Notes in Mathematics*, vol. 57, pp. 1–36, 2006.

[20] H. K. Khalil, *Nonlinear Systems*, Prentice-Hall, Upper Saddle River, NJ, USA, 3rd edition, 2002.

[21] K. H. Guo, N. Li, and Y. Zhuang, "Affecting factors experiment in tire lateral force," *Transactions of the Chinese Society for Agricultural Machinery*, vol. 42, no. 12, pp. 1–5, 2011, in Chinese.

[22] S. H. Strogatz, *Nonlinear Dynamics and Chaos: with Applications to Physics, Biology, Chemistry, and Engineering*, Perseus Books Publishing, New York, NY, USA, 2000.
[23] D. G. Wei, K. Xu, Y. B. Jiang et al., "Hopf bifurcation characteristics of dual-front axle self-excited shimmy system for heavy truck considering dry friction," *Shock and Vibration*, vol. 2015, Article ID 839801, 20 pages, 2015.
[24] X. Liu, W. Chen, and J. S. Zhao, "Overview of influencing factors and engineering solutions," *Automobile Technology*, vol. 1, pp. 20–25, 2017, in Chinese.
[25] S. Li and Y. Lin, "Study on the bifurcation character of steering wheel self-excited shimmy of motor vehicle," *Vehicle System Dynamics*, vol. 44, no. 1, pp. 115–128, 2006.